Partitioning and equilibration of Rb and Sr between silicate melts and aqueous fluids

Manuela Borchert [a,*], Max Wilke [b], Christian Schmidt [b], Karen Rickers [c]

[a] Universität Potsdam, Karl-Liebknecht-Str. 24, 14476 Potsdam-Golm, Germany
[b] Deutsches GeoForschungsZentrum (GFZ), Section 4.1, Telegrafenberg, 14473 Potsdam, Germany
[c] Hamburger Synchrotronstrahlungslabor at Deutsches Elektronensynchrotron, Notkestr. 85, 22607 Hamburg, Germany

ARTICLE INFO

ABSTRACT

Trace element concentrations in aqueous fluids in equilibrium with haplogranitic melt were determined *in situ* at elevated P–T conditions using hydrothermal diamond-anvil cells and synchrotron-radiation XRF microanalyses. Time-resolved analyses showed that the Rb and Sr concentrations in the fluids became constant in less than 2000 s at all temperatures (500 to 780 °C). Although fluid–melt equilibration was very rapid, the change in the concentration of both elements in the fluid with temperature was fairly small (a slight increase for Rb and a slight decrease for Sr). This permitted partitioning data for Rb and Sr between haplogranitic melt and H_2O or $NaCl+KCl+HCl$ aqueous solutions at 750 °C and 200 to 700 MPa to be obtained from EMP analyses of the quenched melt and the *in situ* SR-XRF analyses of the equilibrated fluid. The resulting $D_{Rb}^{f/m}$ and $D_{Sr}^{f/m}$ were 0.01 ± 0.002 and 0.006 ± 0.001 for water as starting fluid, and increased to 0.47 ± 0.08 and 0.23 ± 0.03 for 3.56 m ($NaCl+KCl$) $+0.04$ m HCl at pressures of 224 to 360 MPa. In the experiments with H_2O as starting fluid, the partition coefficients increased with pressure, i.e. $D_{Rb}^{f/m}$ from 0.01 ± 0.002 to 0.22 ± 0.02 and $D_{Sr}^{f/m}$ from 0.006 ± 0.001 to 0.02 ± 0.005 with a change in pressure from 360 to 700 MPa. At pressures to 360 MPa, the Rb/Sr ratio in the fluid was found to be independent of the initial salt concentration (Rb/Sr $= 1.45 \pm 0.6$). This ratio increased to 7.89 ± 1.95 at 700 MPa in experiments with chloride free fluids, which indicates different changes in the Rb and Sr speciation with pressure.

© 2008 Elsevier B.V. All rights reserved.

1. Introduction

Interactions between magmas and aqueous solutions play an important role in many geological processes, e.g., volcanic eruptions, the development of mid-ocean ridges, the formation of magmatic-hydrothermal ore deposits, and crustal metamorphic systems. Equilibria between two or more fluids often result in strong fractionation particularly of trace elements (e.g., Holland, 1972; Rickers et al., 2006). Furthermore, many trace elements are used as petrogenetic indicators in igneous systems (cf., Winter, 2001; Best, 2003). This has prompted several experimental studies on element partitioning at fluid immiscibility conditions over the last 20 years. The trace element partitioning between aqueous fluids and granitic melts was investigated by Flynn and Burnham (1978); London et al. (1988); Keppler and Wyllie (1991); Ayers and Eggler (1995); Adam et al. (1997); and Bai and Koster van Groos (1999). However, systematic studies of fluid–melt partitioning are far from being complete, even for the petrogenetically important large ion lithophile (LIL) elements Rb and Sr. Furthermore, the majority of the experimentally determined partitioning data is based on analyses of quenched samples. However, intrinsic uncertainties are associated with fluid–melt partitioning data from quench techniques, which make it problematic to obtain unambiguous data, particularly for the trace

element concentration in the fluid. The uncertainties are related to (i) the difficulty of isolating the fluid phase for sampling and analysis, (ii) fluid unmixing and (iii) precipitation of solids during quenching, and possible back reactions between fluid and melt during cooling (Holtz et al., 1995; Adam et al., 1997; Behrens et al., 2001).

In this study, we therefore applied a technique to determine the trace element concentration in the fluid phase directly at elevated pressures and temperatures using a modified hydrothermal diamond-anvil cell (HDAC) and synchrotron-radiation X-ray fluorescence microanalysis (SR-µXRF). The first goal of this study is to determine the Rb and Sr concentrations in the fluid *in situ* in equilibrium with a metaluminous melt at 750 °C and 200 MPa. The melt droplets cannot be analysed *in situ* with confidence due to coexcitation of the aqueous fluid around the droplets. Even if the incident beam is focused, a portion of these X-rays will be scattered in the diamond anvil, and a contribution from coexcited fluid to the XRF signal is therefore inevitable if the measurements are done in forward scattering geometry (e.g., Bureau et al., 2007). Such a contribution can be minimised if a recess in the diamond anvil is used and the XRF signal is acquired at 90° to the beam (Schmidt and Rickers, 2003). However, in this experimental setup, it is unlikely that a melt globule occupies the entire effective excitation volume in the recess (cf., Fig. 1 in Muñoz et al., 2005). In this study, electron microprobe (EMP) analyses were therefore performed on the quenched glass droplets after the run. The element contents of the glass and the *in situ* data of the fluid were

* Corresponding author.
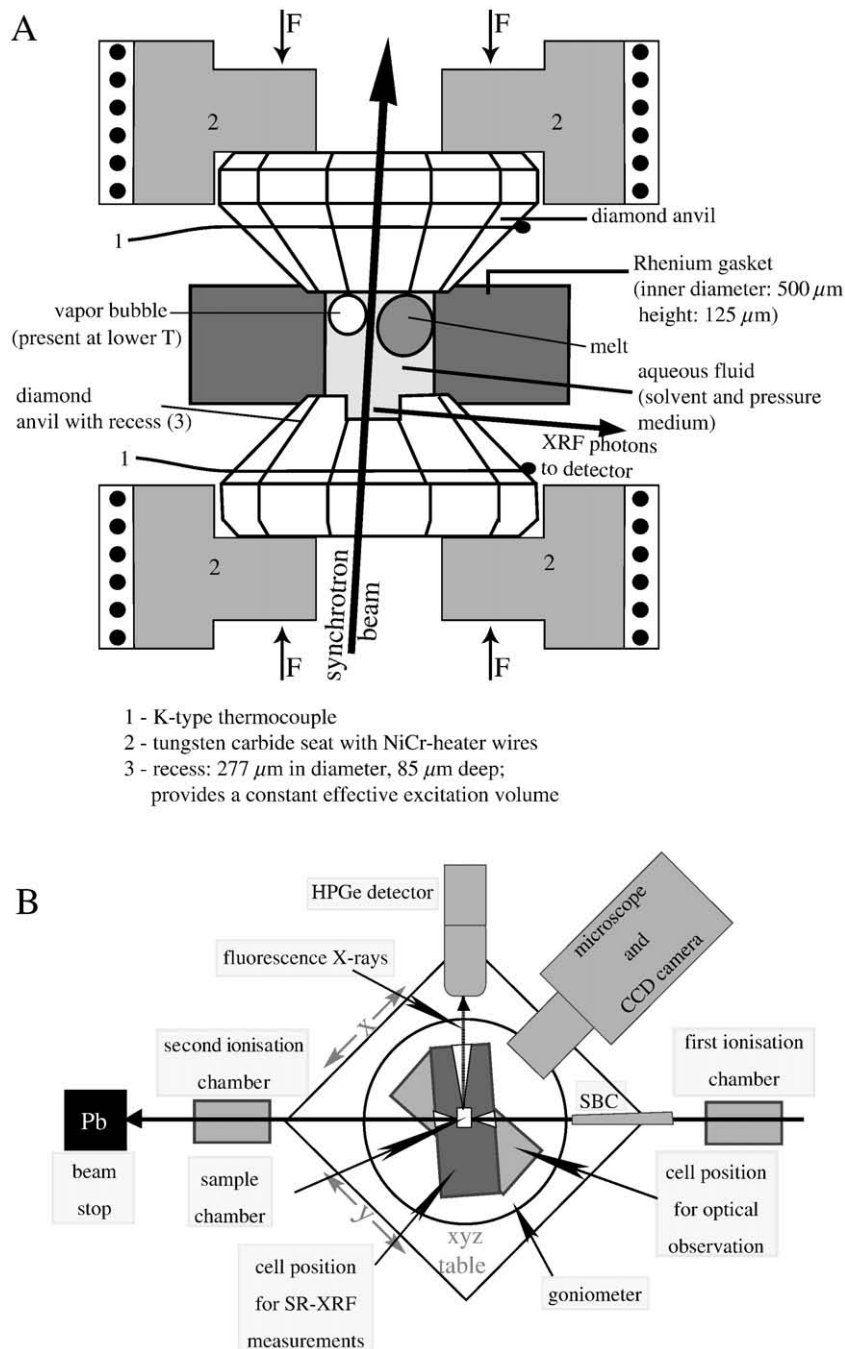*E-mail address:* manu@geo.uni-potsdam.de (M. Borchert).

Fig. 1. A — Schematic diagram showing the details of the modified Bassett-type hydrothermal diamond anvil cell. B — Top view of the experimental setup at beamline L, HASYLAB (DESY, Hamburg) (after Schmidt and Rickers, 2003, SBC - single bounce capillary).

used to obtain partition coefficients. The second goal was to investigate the equilibration kinetics in order to estimate the effect on partition coefficients. This was done by time resolved analysis of the trace element signal in the fluid at several temperatures in stepwise heating and cooling experiments.

2. Experimental methods

2.1. Starting materials

The starting materials for the experimental runs consisted of a synthetic haplogranitic metaluminous glass and two aqueous fluids. The composition of the glass ($Ab_{47}Or_{22}Qz_{31}$) corresponds to the thermal minimum in the haplogranitic system at $P=500$ MPa and

$a_{H_2O}=1$ (Johannes and Holtz, 1996). The glass was prepared in two steps. Firstly, an initial glass was produced using powders of SiO_2, Al_2O_3, Na_2CO_3 and K_2CO_3. The powders were mixed and stepwise heated to 1550 °C for decarbonisation (12 h). After quenching, the glass was crushed and melted again for 48 h at 1550 °C. Secondly, Rb and Sr were added as RbCl and $SrCO_3$ to the crushed initial glass. The glass was doped with relatively high concentrations of 2926 ± 169 ppm Rb and 3065 ± 181 ppm Sr (EMP analyses) to facilitate later *in situ* SR-µXRF analyses of the aqueous fluids. The doped glass powder was melted at 1600 °C for 24 h, then quenched, crushed and melted again for 24 h at 1600 °C to achieve chemical homogeneity. Before loading into the sample chamber of a cell, the glass was cut in pieces with parallel faces. These pieces were ground and polished to a thickness of 60 ± 20 µm.

The solutions, H_2O and $H_2O + 0.5\ m$ NaCl $+ 0.5\ m$ KCl $+ 0.01\ m$ HCl, were produced from distilled de-ionised water, analytical grade powders of NaCl and KCl. A small amount of 30 vol.% hydrochloric acid was added.

2.2. Hydrothermal diamond-anvil cell

We used two modified Bassett-type hydrothermal diamond-anvil cells as described by Bassett et al. (1993), Schmidt and Rickers (2003), and Schmidt et al. (2007). A schematic drawing of this cell type is shown in Fig. 1A. In each cell (HDAC 3 and HDAC G), the culet face of the diamond-anvil located on the side of the incident X-ray beam has a cylindrical recess of 85 μm in depth (HDAC G) or 72 μm in depth (HDAC 3). The recess permits collection of the fluorescence signal at 90° to the incident beam and in the polarisation plane of the beam (Bassett et al., 2000; Schmidt and Rickers, 2003). This configuration minimises the background in the spectra from elastic and Compton scattering and therefore provides an optimal signal to noise ratio. Furthermore, the recess ensures a well-defined effective excitation volume, because fluorescence X-rays generated in other parts of the sample chamber are absorbed by the gasket before reaching the detector. In both cells the path length of the fluorescence X-rays through the diamonds was 460 ± 50 μm. The sample volume was heated externally by NiCr coils around the tungsten carbide seats supporting the anvils. K-type thermocouples attached to the diamonds were used for temperature measurement. The power input to the two resistive heaters was controlled with Eurotherm® 2408 or Eurotherm® 2704 temperature controllers, which kept the temperature within ±0.5 °C of the desired value. The actual temperature in the sample chamber was calibrated using measurements of the melting point of sodium chloride (800.5 °C) at atmospheric pressure and of the triple point of H_2O (0.01 °C). During heating, oxidation of the metallic parts was prevented by flushing the cell with 200 l/h $N_2 + 1\%\ H_2$ gas.

2.3. Sample preparation

The sample chamber of the HDAC consists of the recess at the culet face and a cylindrical hole in the gasket separating the two anvils. Rhenium was selected as gasket material due to its relatively inert behaviour in near neutral aqueous solutions at high temperatures (Xiong and Wood, 2002) and its mechanical properties. The Re gaskets had an initial thickness of 125 μm and a hole diameter of 500 μm. The gasket was mounted on the culet face of the lower diamond anvil and then slightly compressed between the anvils to prevent uncontrolled leakage of the fluid during loading. Then, a glass chip of known dimensions was placed in the sample chamber. The dimensions were chosen such that the glass amount was about 20 to 25 wt.% of the desired bulk composition. This liquid–glass ratio was found to be optimal, because a larger proportion of glass increased the probability that both melt and fluid were present in the recess and thus in the effective excitation volume. A smaller proportion of glass complicated later chemical analyses of the quenched melt droplets due to their small size. The mass of the glass chip was obtained using a density of 2.4 g/cm³ and the volume calculated from the measured dimensions of the glass piece, because the mass of the glass chip was too small for accurate determination by weighing. The aqueous fluid was then transferred into the sample chamber. Before the sample chamber was sealed, an air bubble was allowed to grow by controlled leaking of the liquid. The actual proportion of glass was calculated from the sample chamber volume, the volume of the glass piece calculated from the known dimensions, the glass density, the fluid density obtained from the liquid–vapour homogenisation temperature ($T_H = T_{L+V \to L}$) during first heating, and the salinity. The volume ratio of the produced air bubble to the remaining liquid was chosen such that the fluid density was sufficiently low to attain a pressure between 200 and 500 MPa at 750 °C. After loading, the gasket was slightly compressed further between the anvils, just enough to seal the sample chamber. This procedure minimises the reduction of the sample chamber volume due to gasket flow during first heating. For experiments with salt solutions, the actual salt concentration in the aqueous fluid after sealing was determined from the measured vapour-saturated ice liquidus temperature $T_m = T_{(I+L+V \to L+V)}$, the known ratio of the solutes, and literature data for the vapour-saturated ice liquidus in the system $H_2O + NaCl + KCl$ (Hall et al., 1988).

2.4. HDAC experiments

The loaded cell was fixed on a goniometer on the top of the xyz table at the beamline (Fig. 1B) in the position for optical observation. The cell was heated to measure the T_H of the aqueous fluid, and then to the first experimental temperature. If the excitation volume was free of melt (cf., Fig. 2), the cell was rotated around the vertical axis into the position for XRF spectrum acquisition. The sample chamber was aligned to the beam and the fluorescence detector. The Rb Kα signal was scanned across the recess to verify that the measurement position was correct and that no melt droplet had moved into the recess. Subsequently, XRF spectra of the fluid were acquired as a function of time and with time steps of 500 or 1000 s. After spectrum acquisition, the cell was rotated back to the microscope position, and a new temperature was set. If no melt had entered the recess, the cell was moved back to the XRF position and aligned again. This process took about 5 min. At each P–T condition, consecutive XRF spectra of the fluid were recorded until the XRF signal indicated that equilibrium was attained or that melt had moved into the effective excitation volume. At the end of a stepwise cooling sequence, the cell was heated again to 750 °C and then quenched after attainment of equilibrium with a rate of 200 °C/min. This was done to obtain $D^{f/m}$ values from subsequent EMP analyses of the quenched melt.

During first heating, gasket creep causes a permanent sample volume change (Schmidt and Rickers, 2003). However, the sample volume is nearly constant upon cooling. The actual density of the fluid was therefore determined from measurements of the liquid–vapour homogenisation temperature after each temperature step during stepwise heating. In the case of stepwise cooling, it was measured only after the last temperature step.

For the calculation of density and pressure in experiments with salt solutions, the composition was first simplified by setting wt.% NaCl + wt.% KCl = wt.% (NaCl + KCl). Similar approximations of complex compositions are often used in studies of natural fluid inclusions to model isochores based on the system $H_2O + NaCl$ (Roedder, 1984; Bodnar, 2003). The density was calculated using correlations for the molar volume given by Driesner (2007) for NaCl + H_2O solutions and the equation of state (EOS) by Haar et al. (1984) for pure H_2O based on the determined T_H and wt.% (NaCl + KCl). We used the EOS by Haar et al. (1984) because it is the reference equation of state used by Driesner (2007) for the pure water system. The pressure at the experimental temperature was calculated
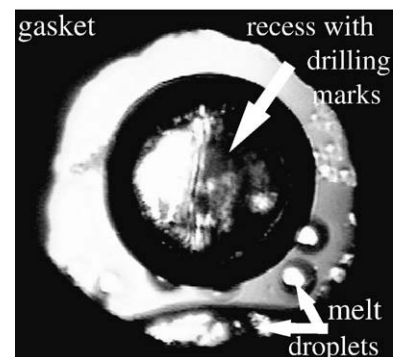

Fig. 2. View into the sample chamber at 750 °C. The recess is free of melt and thus the measured SR-μXRF signal contains no contribution from the melt.
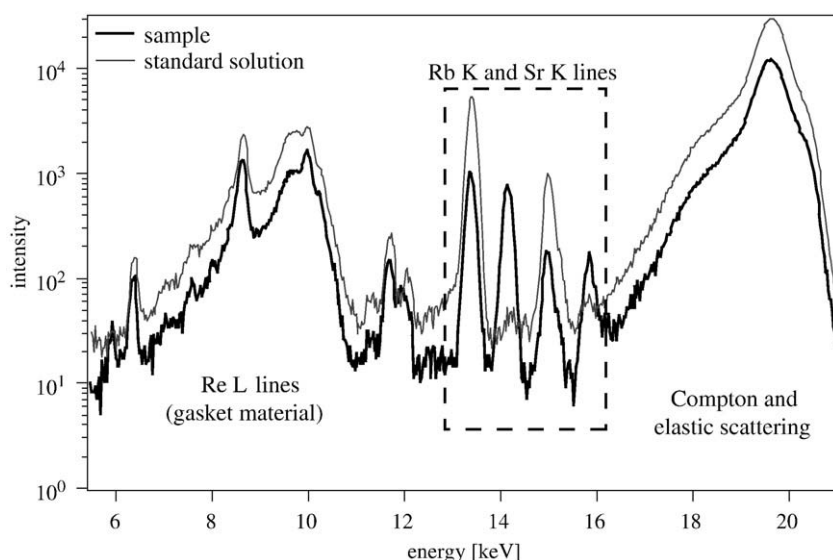
Fig. 3. SR-µXRF spectra of a sample containing 2.84 *m* (NaCl+KCl)+0.03 *m* HCl and a standard solution.

from the salinity expressed as wt.% (NaCl+KCl) and the homogenisation temperature measured after the experiment. The calculations were based on the slopes of the lines of constant T_H given by Bodnar and Vityk (1994) for salt-bearing compositions, and the EOS by Haar et al. (1984) for experiments with H_2O as initial fluid composition. At the conditions of our study, the effect of dissolved silica on pressures based on isochores calculated from T_H is insignificant (Shen et al., 1993). Furthermore, the solubility of melts with high aluminum content in water is low (Mysen and Acton, 1999). Moreover, the iso-T_H line slopes for $H_2O+NaCl$ (Bodnar and Vityk, 1994) are from experiments at SiO_2 saturation. Additionally, the effect of an error in the density on the calculated pressure is much smaller at low densities (such as those in this study) than at high densities. For all these reasons, the pressures calculated here should be sufficiently accurate.

2.5. XRF spectra acquisition and calibration

The experiments were performed at beamline L (HASYLAB) of DORIS III, a second-generation synchrotron light source at DESY, Hamburg, Germany. A single bounce capillary (SBC) was used to focus the synchrotron beam. The capillary was developed and manufactured at Cornell University for the source characteristics of beamline L (Huang and Bilderback, 2006). The SBC has a focal distance of 5 cm and focuses hard X-rays up to 40 keV into a spot of 11 ± 1 µm. A micro-beamstop was aligned at the beam entrance into the SBC to absorb the portion of beam that would pass the capillary without focusing. Utilisation of the SBC increases the flux density by a factor of 300, and therefore decreases the lower limit of detection for elements with fluorescence energies between 12 and 20 keV to 1 to 5 ppm in HDAC experiments (Schmidt et al., 2007). In this study, the lower limit of detection of Rb was 1 to 2 ppm, as determined from SR-µXRF spectra of standard solutions loaded into HDAC 3 and HDAC G. The lower limit of detection (*mdl*) was calculated from $mdl = 3c\sqrt{B}/I$, where *c* is the concentration, *B* the background intensity and *I* the peak intensity (e.g., Haller and Knöchel, 1996).

A synchrotron beam with a photon energy of 20.3 ± 0.1 keV provided by a multilayer wide bandpass monochromator was used for excitation. All XRF spectra were recorded using a high purity Ge solid-state detector aligned in the polarisation plane of the incoming X-rays at 90° to the synchrotron beam. The spectra were collected with live counting times of 500 or 1000 s.

Fig. 3 shows two examples of obtained XRF spectra, one of a standard solution and the other one of an aqueous fluid in equilibrium with melt at 750 °C. The integrated intensities of the fluorescence lines

were obtained from fits of the spectra using PyMca, a graphical interface for multi-channel analyser spectra visualisation and analysis developed at the ESRF (Solé et al., 2007). The integrated intensities were normalised to the intensity of the incident beam and then divided by the density of the fluid. The normalised integrated intensities were calibrated using XRF spectra of standard solutions. The standard solutions had initial concentrations of 250 and 995 ppm Rb (matrix 10 wt.% NaCl). Before the sample chamber is sealed, a small portion of the H_2O of the solution evaporates, which increases the NaCl and Rb concentration. Therefore, the actual concentration of Rb in the standard solution after loading into the sample chamber was determined from the actual NaCl concentration calculated from the measured vapour-saturated ice melting temperature, and the known NaCl/RbCl ratio ($c_{actual}^{Rb} = c_{initial}^{Rb} * c_{actual}^{NaCl} / c_{initial}^{NaCl}$). For each cell, two XRF spectra were collected at temperatures slightly above T_H. The obtained integrated intensities of the Rb K fluorescence lines of the standard solutions were normalised to the intensity of the incident beam and divided by the fluid density. The Sr concentration in the fluid was determined based on normalisation of the integrated intensities of the Sr K fluorescence lines to the density of the fluid and the intensity of the incoming beam, the calibration for Rb from the standard solutions, and multiplication with a Rb/Sr correction factor. This factor corrects for different cross-sections of the Rb and Sr K fluorescence and fluorescence transmission through the diamond. A Rb/Sr correction factor of 0.844 ± 0.006 was obtained for HDAC 3 from XRF spectra of a standard solution with equal concentrations of Rb and Sr (500 ppm each) loaded into the sample chamber. These spectra were collected using the same procedure as described above. The empirical Rb/Sr factor differs only by 2% from the theoretical value calculated by multiplying the ratio of the fluorescence-cross sections (e.g., XRAYLIB, Brunetti et al., 2004) with the ratio of the transmission of the K line fluorescence X-rays through 0.5 mm diamond. This small difference is within the uncertainties of the databases (e.g., Brunetti et al., 2004). We also applied the empirical Rb/Sr correction factor to the spectra from experiments using HDAC G, because the design of both cells and the X-ray path length were very similar.

2.6. EMP analyses

After quenching, the glass droplets in the gasket were embedded in epoxy resin, ground and polished. The EMP measurements were carried out at the GFZ Potsdam using a CAMECA SX-100. The analysed elements were Na, K, Al, Si, Rb and Sr. The measurement conditions

Table 1
Summary of the experimental conditions, results of the *in situ* SR-μXRF analyses of the aqueous fluids, and of the EMP analyses of the glasses, and calculated partition coefficients ($D^{fluid/melt} = c^{fluid}/c^{melt}$) at 750 °C

Sample	1	2	3	4	5
Cell	HDAC 3	HDAC 3	HDAC G	HDAC G	HDAC G
P_{exp} at $T_{exp}=750$ °C [MPa]	224	262	360	540	700
m (NaCl+KCl)	3.56	2.84	0	0	0
m HCl	0.04	0.03	0	0	0
NaCl+KCl [wt.%]	16.8	14.3	0	0	0
% glass [wt.%]	24	17	24	23	35
ρ_{fluid} [g/cm³]	0.6855	0.6940	0.6336	0.7494	0.8022
T_m [°C]	−10.6	−8.6	n.d.	n.d.	n.d.
T_H [°C]‡	439	409	333	281	248
c_{Rb}^f [ppm]	712±6	308±4	31±5	77±6	546±42
c_{Rb}^m [ppm]	1510±247	1028±224	3007±275	n.d.*	2487±172
c_{Sr}^f [ppm]	495±6	205±3	22±3	19±3	69±16
c_{Sr}^m [ppm]	2085±299	1663±333	3532±555	n.d.*	3270±142
$\frac{c_{Rb}^f}{c_{Sr}^f}$	1.44±0.02	1.51±0.03	1.39±0.15	4.16±0.42	7.89±1.59
$D_{Rb}^{f/m}$	0.47±0.08	0.30±0.07	0.01±0.002	n.d.*	0.22±0.02
$D_{Sr}^{f/m}$	0.24±0.03	0.12±0.02	0.006±0.001	n.d.*	0.02±0.005
SiO₂ [wt.%]	73.37	71.51	73.89	n.d.*	68.74
Al₂O₃ [wt.%]	12.77	12.37	12.81	n.d.*	13.64
Na₂O [wt.%]	3.49	2.82	4.25	n.d.*	2.58
K₂O [wt.%]	5.72	6.14	3.39	n.d.*	3.93
ASI	1.07	1.10	1.20	n.d.*	1.33

The listed element concentrations in the fluid and melt represent average values. ^{f} — fluid; ^{m} — melt; m — molality; n.d. — not determined; % glass — proportion of glass; ‡ — measured after collection of XRF spectra at $T_{exp}=750$ °C; ASI = $\frac{Al_2O_3}{Na_2O+K_2O}$ in moles; n.d.* — not determined because sample was lost during preparation for EMP analysis.

were a beam current of 10 nA, an electron beam energy of 15 keV, and counting times of 10 s for Na and K, 20 s for Al and Si, and 30 s for Rb and Sr.

3. Results and discussion

The experimental conditions, the Rb and Sr concentrations in the fluids coexisting with melt obtained from *in situ* SR-μXRF analyses, the results of the EMP analyses of the glasses after the quench, and the calculated D values are listed in Table 1. Fig. 4 shows the Rb and Sr concentrations in the aqueous fluid coexisting with melt at different temperatures for 3 different initial fluid compositions as a function of the time elapsed after the run temperature was reached. The results of both the stepwise heating and cooling runs indicate rapid equilibration of Rb and Sr between fluid and melt in all experiments. For chloridic fluids (Fig. 4A and B), equilibrium was attained in less than 2000 s. If the random error in the concentrations is taken into account, it is very likely that equilibration was faster than the minimum time required to complete acquisition of the first XRF spectrum (about 500 s). For chloride-free fluids (Fig. 4C), the time required to reach equilibrium at 750 °C was probably below 3000 s, but this is difficult to constrain from the data due to the relatively large error in the concentrations. We believe that the trace element concentrations in the fluids obtained in this study represent equilibrium values. Our data show stable Rb and Sr concentrations over a relatively long time at T_{exp}, e.g., over 9000 s in the experiment with H₂O as starting fluid shown in Fig. 4C. Furthermore, the existence of a significant concentration gradient in the aqueous phase in the recess at high temperatures is very unlikely because convection in the sample chamber is substantial and diffusion is rapid. This is supported by a study on rutile dissolution in aqueous fluids using a HDAC (Audétat and Keppler, 2005), in which a diffusion coefficient of 8.0×10^{-7} m²s⁻¹ at 800 °C and 2 GPa was calculated assuming a hydrated complex of Ti⁴⁺. This diffusion coefficient translated into a travel time of the complex of about 0.16 s across the entire sample chamber of 500 μm in diameter. In analogy to silicate melts (Koepke and Behrens, 2001), Rb and Sr diffusion in aqueous fluids can be expected to be even faster than the diffusion of this high-field strength element.

The Rb and Sr concentrations in the fluid can be directly compared for experiments with similar glass/fluid ratios and pressures (Table 1). The concentrations of both elements increased by an order of magnitude with addition of chloride to the starting fluid (from 0 to 3.56 m (NaCl+KCl)+ 0.04 m HCl) due to their affinity to form Cl complexes in aqueous solutions.

The temperature dependence of the Rb and Sr concentrations in chloridic fluids shows opposite trends along an isochore, i.e., slightly decreasing Rb contents and slightly increasing Sr concentrations upon cooling. This is more pronounced for the experiment containing 3.56 m (NaCl+KCl)+0.04 m HCl in the starting fluid (Fig. 4A). The Rb concentration in the fluid decreased by 17% from 737±12 to 611±1 ppm upon cooling from 780 to 600 °C, whereas the Sr content increased by 12% from 473±8 to 531±10 ppm. The same trends were also recognisable, but less distinct, in the experiment with an initial salinity of 2.84 m (NaCl+KCl)+ 0.03 m HCl (Fig. 4B). In this experiment, there may also have been a small pressure effect on the Sr content in the fluid at 680 °C (232±8 ppm at 160 MPa and 212±8 ppm at 212 MPa), while the Rb concentration remained constant at 305±8 ppm.

In the experiment at 360 MPa with H₂O as initial fluid (Fig. 4C), XRF spectra were collected only at 750 °C. The average concentrations were 31±5 ppm Rb and 22±3 ppm Sr. Due to the low concentrations, the error was too large to obtain concentration changes along an isochore with confidence. At 750 °C, the Rb concentration in the fluid increased with pressure by a factor of about 2.5 from 31±5 ppm at 360 MPa to 77±6 ppm at 540 MPa for similar glass/fluid ratios. In contrast, the Sr concentration remained nearly constant (22±3 ppm at 360 MPa and 19±3 ppm at 540 MPa). The increase in the Rb concentration may indicate that the pH of the aqueous fluid becomes more basic, which would suggest that Rb complexes predominantly with OH in the absence of ligands such as Cl. Such a change in pH could be related to the enhanced water dissociation (Bandura and Lvov, 2006) and an enhanced water–melt reaction with pressure (e.g., Stalder et al., 2000). The latter may involve formation of alumosilicate complexes in the fluid, as suggested by e.g., Manning (2004), and Manning (2007) for high pressures. In contrast, the nearly constant Sr concentration suggests a significant difference in the complexation of Sr compared to that of Rb.

The difference in the pressure dependence of Rb and Sr becomes even more obvious if the Rb/Sr ratio in the fluid is considered. Fig. 5 shows the Rb/Sr ratio in the fluid as a function of pressure and initial fluid salinity. At pressures between 224 and 360 MPa, the Rb/Sr ratio was independent of the initial salt concentration, with a Rb/Sr value of 1.45± 0.06. In contrast, an increase of the Rb/Sr ratio with pressure was observed in the case of the experiments with H₂O, up to a ratio of 7.89± 1.95 at 700 MPa. This strong change of the Rb/Sr ratio with pressure points to different trends of the speciation of the two elements in Cl-free aqueous fluids.

The relationship between the calculated fluid–melt partition coefficients $D^{f/m}$ ($D^{f/m}=c^f/c^m$, where c^f is the concentration in the fluid and c^m is the concentration in the melt) and the initial salt concentration of the fluid is illustrated in Fig. 6. The fluid–melt partition coefficients of Rb and Sr were determined for different salinities at 750 °C and 220 to 700 MPa. We observed a positive correlation of the $D^{f/m}$ values with initial chlorinity of the fluid. The $D_{Rb}^{f/m}$ increased from 0.01 for H₂O as initial fluid to 0.47 for a 3.56 m (NaCl+KCl)+0.04 m HCl. The $D_{Sr}^{f/m}$ were slightly smaller and changed from 0.006 to 0.24. The effect of pressure on the partition coefficients appears to be smaller compared to that of the salinity. For H₂O experiments, the $D^{f/m}$ increased from 0.01 to 0.22 (Rb) and 0.006 to 0.02 (Sr) for a pressure increase from 360 to 700 MPa.

Fluid/melt partitioning of Rb and Sr was previously studied by Bai and Koster van Groos (1999) and Webster et al. (1989) using conventional quench experiments. The $D^{f/m}$ obtained by Bai and Koster van Groos (1999) are much higher in the case of chloride-bearing systems. For similar P–T conditions, they reported a $D_{Rb}^{f/m}$ of 1.56 and a $D_{Sr}^{f/m}$ of 0.94 at
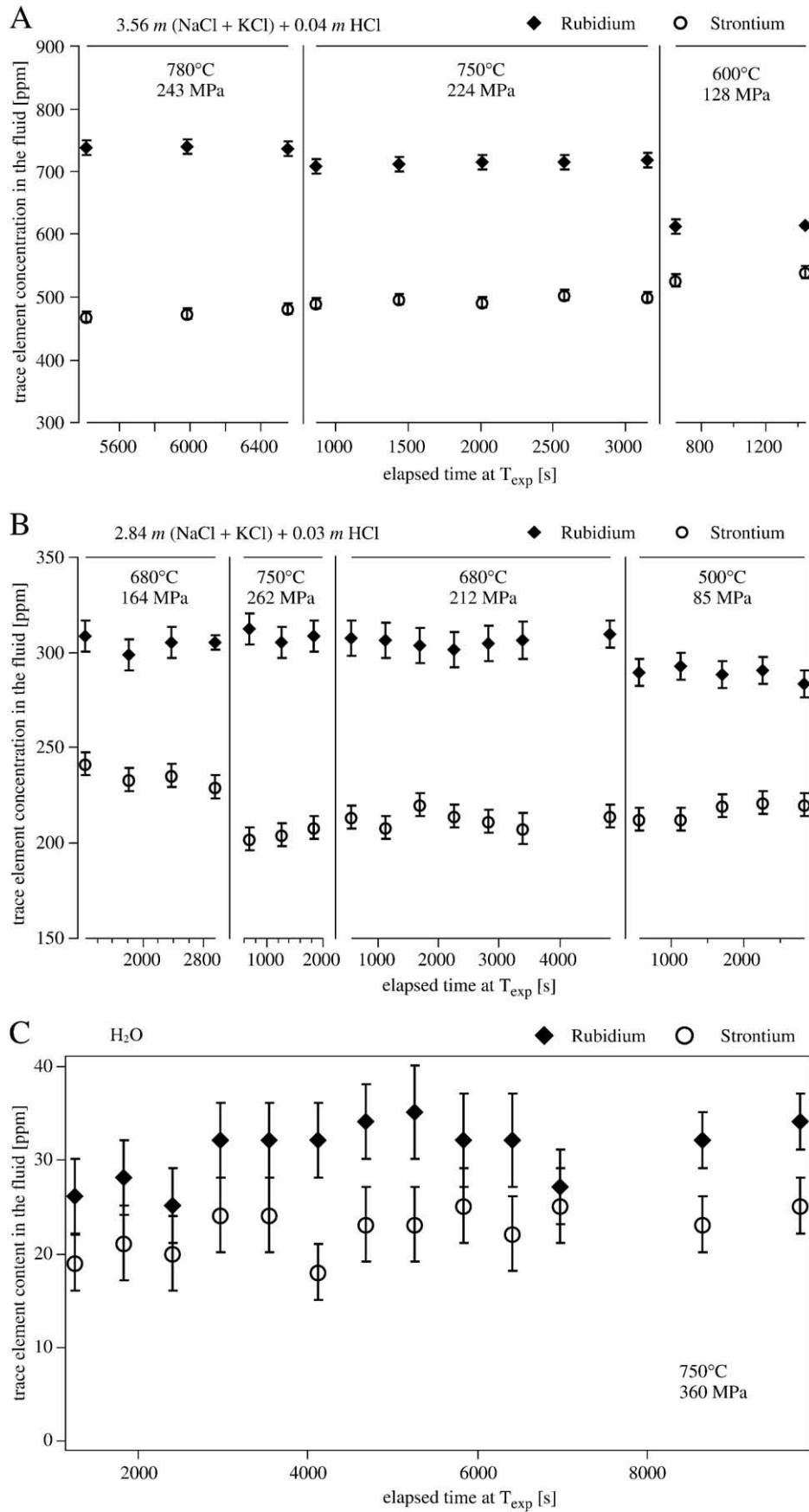
Fig. 4. Concentration of trace elements Rb and Sr in the aqueous fluid vs. elapsed time after attainment of the experimental temperature T_{exp} for various fluid compositions: A − 3.56 m (NaCl+KCl)+0.04 m HCl, **B** − 2.84 m (NaCl+KCl)+0.03 m HCl and, **C** - H_2O. The error bars represent 2σ errors.
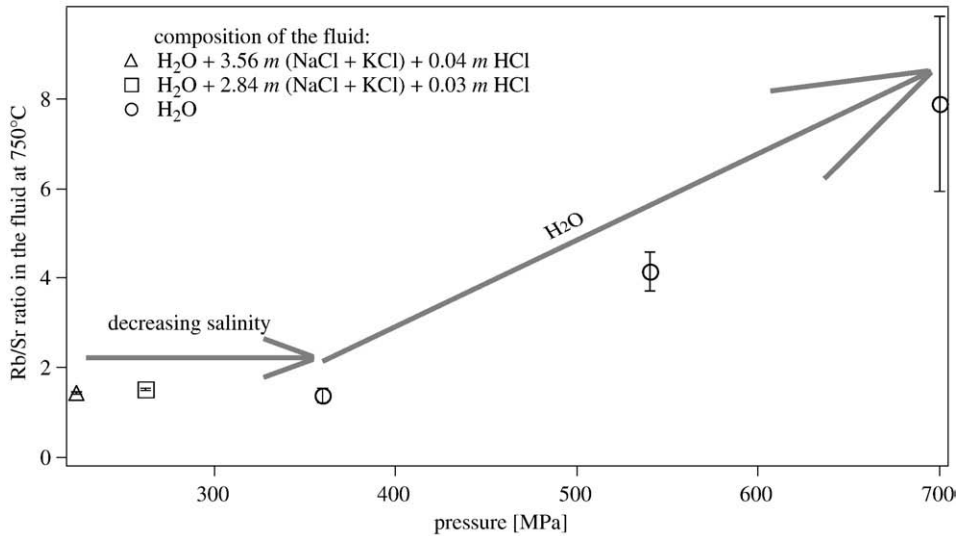
Fig. 5. Rb/Sr ratio in the fluid at 750 °C vs. pressure. At low pressures, the Rb/Sr ratio was constant for the studied compositions. A strong increase in the Rb/Sr ratio in the fluid with pressure was observed for H$_2$O+melt experiments.

750 °C and 200 MPa. This differs from our results by a factor of 3.3 for Rb and 4 for Sr. However, Bai and Koster van Groos (1999) used a different initial fluid composition (1.3 m NaCl+2.9 m KCl), which also resulted in other melt compositions due to the exchange of sodium and potassium between melt and fluid. Webster et al. (1989) provided data at about 770 °C and 200 MPa for H$_2$O+HCl+melt systems. For two experiments differing only in the run duration, they reported quite different $D_{Rb}^{f/m}$ of 0.3 and 1.4. The lower value is similar to those obtained in this study at much higher Cl concentrations. This suggests that addition of HCl (and thus lowering the pH) causes a higher partitioning of Rb into the fluid than addition of NaCl+KCl. However, the large variation in the results for the 2 runs reported by Webster et al. (1989) could also be related to experimental difficulties in quench experiments (see Introduction). For Sr, only one value was obtained ($D_{Sr}^{f/m}$=0.1), which differs similarly from our results as those for Rb.

Bai and Koster van Groos (1999) provided data from melt+H$_2$O experiments at 750 °C and 200 MPa. The reported partition coefficients of Rb (0.006) and Sr (0.002) are much lower than those at 360 MPa obtained in this study ($D_{Rb}^{f/m}$=0.01 and $D_{Sr}^{f/m}$=0.006 at

750 °C). The experiments from both studies were at similar compositions but differed in pressure by 160 MPa, which can only in part explain the discrepancies in the $D^{f/m}$.

4. Conclusions

The technique successfully applied in this study has two important advantages. The trace element concentration in the fluid can be determined without the ambiguities associated with data from quench techniques. Additionally, kinetic information can be obtained. The drawbacks are, however, limited availability of beam time and a more difficult control of the bulk composition and pressure, which complicates systematic studies.

The technique can be improved further by the following. (i) The experimental setup can be modified for permanent optical observation of the sample chamber, which would allow to study the equilibration process at shorter timescales. This is because no time is lost to rotate and align the cell before acquisition of XRF spectra. Another advantage is permanent visual monitoring of the effective
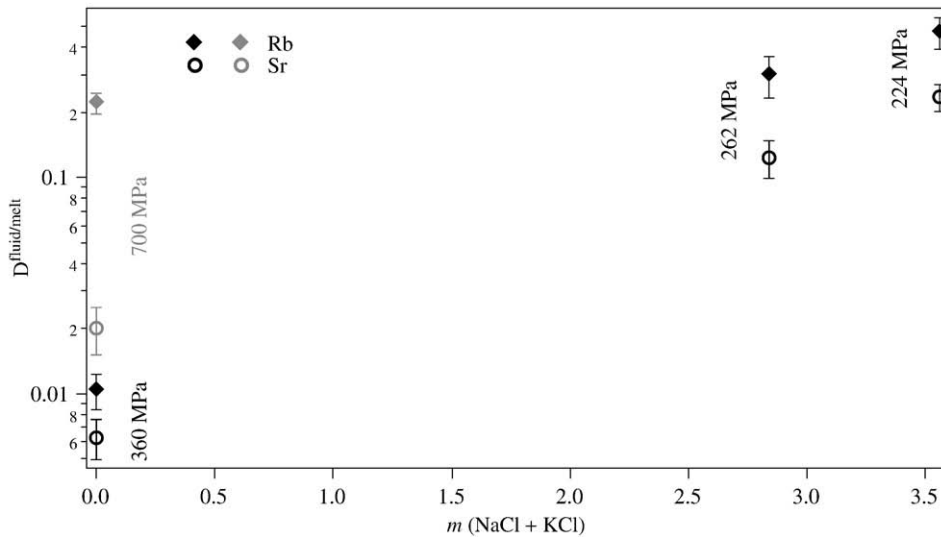

Fig. 6. Fluid–melt partition coefficients of Rb and Sr vs. initial salt concentration of the fluid [m (NaCl+KCl)] at 750 °C. For similar pressures, an increase in the initial salt concentration corresponds to an increase in the $D_{Rb}^{f/m}$ and $D_{Sr}^{f/m}$. For H$_2$O+melt experiments, we observed a pressure dependence of the D values particularly for Rb (light grey symbols = experiment at 700 MPa).

excitation volume, e.g., for immediate recognition of the unwanted case that melt droplets migrate into this volume. (ii) Use of a synchrotron radiation source with higher intensity such as an undulator insertion device will improve the sensitivity and thus the data at low concentrations. In addition, spectrum acquisition times can be reduced, which results in a better temporal resolution in kinetic studies. (iii) The trace element concentration in the glasses can be obtained more accurately using techniques with a higher sensitivity, e.g., using laser-ablation inductively-coupled plasma mass spectrometry, especially if an appropriate element is used as an internal standard, such as Si known from the EMP analyses. (iv) It may be possible to modify the geometry of the anvils and the gasket in such a way that both aqueous fluid and melt can be unambiguously analysed *in situ* in the same experiment at high PT.

The results of this study show, firstly, an increase in the concentrations of Rb and Sr in the fluid by an order of magnitude with addition of chloride to the starting fluid (from 0 to 3.56 m (NaCl+KCl)+0.04 m HCl). Secondly, opposite trends were observed for the temperature dependence of Rb and Sr in the fluid along an isochore. The Rb content in the fluid increased but the Sr concentration decreased with temperature. Thirdly, the Sr concentration in the fluid displayed a slightly negative correlation with pressure at constant temperature, while the Rb content did not change (see Fig. 4B). Furthermore, we observed differences in the pressure dependence of the Rb and Sr concentrations in the fluid in H$_2$O+melt experiments. The Rb/Sr ratio in the fluid increased from 1.45±0.06 to 7.89±1.95 with an increase in pressure from 360 to 700 MPa. The obtained partition coefficients of both elements are positively correlated with the initial Cl concentration of the fluid. In the H$_2$O+melt experiments, we found an increase of the D values with pressure, which was more pronounced for Rb.

The results of this study demonstrate that the equilibration between aqueous fluid and melt is rapid and can therefore affect partition coefficients obtained in quench experiments. However, the observed concentration changes upon isochoric cooling were relatively small. Therefore, these changes can only account for a small portion of the differences between the fluid–melt partitioning data from quench techniques and those obtained in this study. Consequently, uncertainties in the fluid–melt partitioning data from quench techniques can mainly be attributed to the difficulty of obtaining a representative sample of the fluid. Usually, the fluid composition has to be reconstructed from the quenched products (fluid and quench precipitates). As already pointed out by Webster et al. (1989), this may be a major contribution to the error in these experiments and thus explain the often wide spread in the results of runs at similar conditions. This becomes particularly obvious if data from different studies are compared. For example, $D^{f/m}$ reported by Bai and Koster van Groos (1999) at low HCl concentrations are significantly lower (up to a factor of 7.5 for Rb) than those obtained by Webster et al. (1989) at similar conditions. Part of this discrepancy can probably be attributed to the different experimental procedures used to obtain the partition coefficients, and the related systematic error. Therefore, the *in situ* technique applied here can be helpful to obtain more reliable and consistent data on the trace element distribution between aqueous fluid and granitoid melts.

Acknowledgements

References

Adam, J., Green, T.H., Sie, S.H., Ryan, C.G., 1997. Trace element partitioning between aqueous fluids, silicate melts and minerals. Eur. J. Mineral. 9, 569–584.

Audétat, A., Keppler, H., 2005. Solubility of rutile in subduction zone fluids, as determined by experiments in the hydrothermal diamond anvil cell. EPSL, 232, 393–402.

Ayers, J.C., Eggler, D.H., 1995. Partitioning of elements between silicate melt and H$_2$O-NaCl fluids at 1.5 and 2.0 GPa pressure: implications for mantle metasomatism. Geochim. Cosmochim. Acta 59, 4237–4246.

Bai, T.B., Koster van Groos, A.F., 1999. The distribution of Na, K, Rb, Sr, Al, Ge, Cu, W, Mo, La and Ce between granitic melts and coexisting aqueous fluids. Geochim. Cosmochim. Acta 63, 1117–1131.

Bandura, A.V., Lvov, S.N., 2006. The ionization constant of water over a wide range of temperatures and densities. J. Phys. Chem. Ref. Data 35, 15–30 (cf., www.iapws.org).

Bassett, W.A., Shen, A.H., Bucknum, M., Chou, I.-M., 1993. A new diamond anvil cell for hydrothermal studies to 2.5 GPa and from −190 to 1200 °C. Rev. Sci. Instrum. 64, 2340–2345.

Bassett, W.A., Anderson, A.J., Mayanovic, R.A., Chou, I.-M., 2000. Modified hydrothermal diamond anvil cells for XAFS analyses of elements with low energy absorption edges in aqueous solutions at sub- and supercritical conditions. Z. Kristallogr. 215, 711–717.

Behrens, H., Meyer, M., Holtz, F., Benne, D., Novak, M., 2001. The effect of alkali ionic radius, temperature, and pressure on the solubility of water in MAlSi$_3$O$_8$ melts M= (Li, Na, K, Rb). Chem. Geol. 174, 275–289.

Best, M.G., 2003. Igneous and Metamorphic Petrology. Blackwell Publishing. p. 40.

Bodnar, R.J., 2003. Introduction to aqueous fluid systems. In: Samson, I., Anderson, A., Marshall, D. (Eds.), Fluid Inclusions: Analysis and Interpretation, Mineral. Assoc. Canada, Short Course, 32, pp. 81–99.

Bodnar, R.J., Vityk, M.O., 1994. Interpretation of microthermometric data for H$_2$-NaCl fluid inclusions. Fluid Inclusions in Minerals: Methods and Applications. Virginia Tech, Blacksburg, VA, pp. 117–130.

Brunetti, A., Sanchez del Rio, M., Golosio, B., Simionovici, A., Somogyi, A., 2004. A library for X-ray-matter interaction cross sections for X-ray fluorescence applications. Spectrochim. Acta B 59, 1725–1731.

Bureau, H., Ménez, B., Malavergne, V., Somogyi, A., Simionovichi, A., Massare, D., Khodja, H., Daudin, L., Gallien, J.-P., Shaw, C., Bonnin-Mosbah, M., 2007. *In situ* mapping of high-pressure fluids using hydrothermal diamond anvil cells. High Press. Res. 27, 235–247.

Driesner, T., 2007. The system H$_2$O-NaCl. Part II: correlations for molar volume, enthalpy, and isobaric heat capacity from 0 to 1000 °C, 1 to 5000 bar, and 0 to 1 X$_{NaCl}$. Geochim. Cosmochim. Acta 71, 4902–4919.

Flynn, R.T., Burnham, C.W., 1978. An experimental determination of rare earth partition coefficients between a chloride containing vapor phase and silicate melts. Geochim. Cosmochim. Acta 42, 685–701.

Haar, L., Gallagher, J.S., Kell, G.S., 1984. NBS7NRC Steam tables: Thermodynamic and Transport Properties and Computer Programs for Vapor and Liquid States of Water in SI Units. Hemisphere Pub. Corp., Washington, D.C. pp 320.

Hall, D.H., Sterner, S.M., Bodnar, R.J., 1988. Freezing point depression of NaCl-KCl-H$_2$O solutions. Econ. Geol. 83, 197–202.

Haller, M., Knöchel, A., 1996. X-ray fluorescence analysis using synchrotron radiation (SRXRF). J. Trace Microprobe Tech. 14, 461–488.

Holland, H.D., 1972. Granites, solutions, and base metal deposits. Econ. Geol. 67, 281–301.

Holtz, F., Behrens, H., Dingwell, D.B., Johannes, W., 1995. H$_2$O solubility in haplogranitic melts: compositional, pressure, and temperature dependence. Am. Mineral. 80, 94–108.

Huang, R., Bilderback, D.H., 2006. Single-bounce monocapillaries for focusing synchrotron radiation: modeling, measurements and theoretical limits. J. Synchrotron Rad. 13, 74–84.

Johannes, W., Holtz, F., 1996. Petrogenesis an Experimental Petrology of Granitic Rocks. Springer, Berlin. p 40.

Keppler, H., Wyllie, P.J., 1991. Partitioning of Cu, Sn, Mo, W, U and Th between melt and aqueous fluid in the systems haplogranite-H$_2$O-HCl and haplogranite-H$_2$O-HF. Contrib. Mineral. Petrol. 109, 139–150.

Koepke, J., Behrens, H., 2001. Trace element diffusion in andesitic melts: an application of synchrotron X-ray fluorescence analysis. Geochim. Cosmochim. Acta 65, 1481–1489.

London, D., Hervig, R.L., Morgan IV, G.B., 1988. Melt-vapor solubilities and elemental partitioning in peraluminous granite-pegmatite systems: experimental results with Macusani glass at 200 MPa. Contrib. Mineral. Petrol. 99, 360–373.

Manning, C.E., 2004. The chemistry of subduction-zone fluids. EPSL 223, 1–16.

Manning, C.E., 2007. Solubility of corundum+kyanite in H$_2$O at 700 °C and 10 kbar: evidence for Al-Si complexing at high pressure and temperature. Geofluids 7, 258–269.

Muñoz, M., Bureau, H., Malavergne, B., Wilke, M., Schmidt, C., Simionovici, A., Somogyi, A., Farges, F., 2005. *In situ* speciation of nickel in hydrous melts exposed to extreme conditions. Physica Scripta 115, 921–922.

Mysen, B.O., Acton, M., 1999. Water in H$_2$O-saturated magma-fluid systems: solubility behavior in K$_2$O-Al$_2$O$_3$-SiO$_2$-H$_2$O to 2.0 GPa and 1300 °C. Geochim. Cosmochim. Acta 63, 3799–3815.

Rickers, A., Thomas, R., Wilhelm, H., 2006. The behavior of trace elements during the chemical evolution of the H$_2$O-, B-, and F-rich granite-pegmatite hydrothermal system at Ehrenfriedersdorf, Germany: a SXRF study of melt and fluid inclusions. Mineral. Depos. 41, 229–245.

Roedder, E., 1984. Fluid Inclusions. Rev. Mineral. 12. Mineralogical Society of America, Washington, D.C.

Schmidt, C., Rickers, K., 2003. *In-situ* determination of mineral solubilities in fluids using a hydrothermal diamond-anvil cell and SR-XRF: solubility of AgCl in water. Am. Mineral. 88, 288–292.

Schmidt, C., Rickers, K., Bilderback, D.H., Huang, R., 2007. *In situ* synchrotron-radiation XRF study of REE phosphate dissolution in aqueous fluids to 800 °C. Lithos 95, 87–102.

Shen, A.H., Bassett, W.A., Chou, I.-M., 1993. The α-β quartz transition at high temperatures and pressures in a diamond-anvil cell by laser interferometry. Am. Mineral. 78, 694–698.

Solé, V.A., Papillon, E., Cotte, M., Walter, P., Susini, J., 2007. A multiplatform code for the analysis of energy-dispersive X-ray fluorescence spectra. Spectrochim. Acta B 62, 63–68.

Stalder, R., Ulmer, P., Thompson, A.B., Günther, D., 2000. Experimental Approach to constrain second critical end points in fluid/silicate systems: near-solidus fluids and melts in the system albite-H_2O. Am. Mineral. 85, 68–77.

Xiong, Y., Wood, S.A., 2002. Experimental determination of the hydrothermal solubility of ReS_2 and the Re-ReO_2 buffer assemblage and transport of rhenium under supercritical conditions. Geochem. Transactions 3, 1–10.

Webster, J.D., Holloway, J.R., Hervig, R.L., 1989. Partitioning of lithophile elements between H_2O and $H_2O+ CO_2$ fluids and topaz rhyolite melt. Econ. Geol. 84, 116–134.

Winter, J.D., 2001. An Introduction to Igneous and Metamorphic Petrology. Prentice Hall, New Jersey. p. 160.